ACS APPLIED ENERGY MATERIALS

www.acsaem.org Article

Mixed Solvent Engineering for Morphology Optimization of the Electron Transport Layer in Perovskite Photovoltaics

SungWon Cho, Padmini Pandey, Jinwoo Park, Tae-Woo Lee, and Dong-Won Kang*

Cite This: https://doi.org/10.1021/acsaem.1c02913 Read Online

ACCESS | Metrics & More | Article Recommendations | Supporting Information

ABSTRACT: The interfacial charge transport dynamics in perovskite solar cells (PSCs) play a significant role for achieving improved device efficiency. We have shown here the morphology optimization of the electron transport layer (ETL), i.e., [6,6]-phenyl-C61-butyrate methyl ester (PCBM), through solvent engineering by introducing a mixed solvent system (chlorobenzene (CB) and dichlorobenzene (DCB)) in PCBM layer fabrication. The results showed an improvement in morphology and better film coverage with reduced surface roughness and pinholes in ETL by replacing half of CB with a high boiling point solvent in the $CB_{0.5}$−$DCB_{0.5}$ system. Strong quenching in steady-state photoluminescence (PL) indicates that an improved interaction in the perovskite/ETL interface leads to efficient charge transfer, which has been further realized through time-resolved PL (TR-PL) measurement with reduced lifetime τ_{avg} ~2.35 ns. The power conversion efficiency (PCE) in PSCs improved from 17.2% for $CB_{1.0}$−DCB_0 to 18.46% for $CB_{0.5}$−$DCB_{0.5}$ mixed solvent treated ETL. Furthermore, this mixed solvent processing for ETL strengthened the perovskite/ETL interface and minimized the charge carrier recombination, which seems to be a convenient mixed solvent strategy for high-performance PSCs.

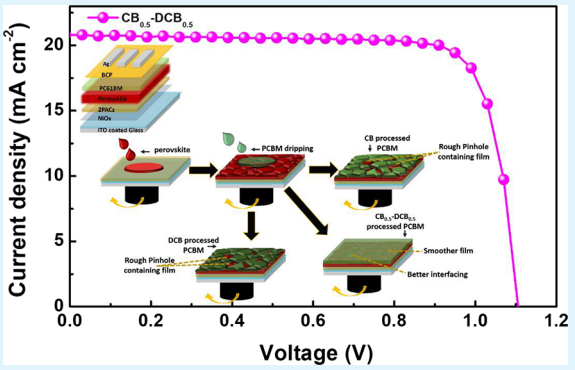

KEYWORDS: *perovskite solar cells, electron transport layer, mixed solvent, chlorobenzene, dichlorobenzene*

INTRODUCTION

Organic−inorganic halide perovskites (OIHPs) have been widely used in recent years in several optoelectronic devices owing to their tremendous properties such as defect tolerance, bandgap tunability, low exciton binding energy, high charge carrier mobility, high molar extinction coefficient, etc.[1−4] OIHPs are efficient photo-absorbers for PSCs and reached an excellent efficiency of 25.5% in PSCs.[5] The scientific fraternity has been constantly putting its efforts in developing high power conversion efficiency (PCE) PSCs by developing several optimizations through tailoring the physical and optical properties of photo-absorbers. As per the S−Q limit model, the theoretical PCE in single junction PSCs is ~33%;[5] however, at the experimental level, there are several factors responsible for efficiency loss in OIHPSCs.[6,7] Additionally, the morphologies of the OIHP and transport layers play crucial roles in the PSC performance.[8−12] The morphology of photo-absorbers is generally related to the light-harvesting and charge carrier generation in PSCs. For boosting PCE in PSCs, there has been broad research going on to fabricate controlled perovskite films with uniformity through solution processing that includes solvent vapor annealing, sequential depositions, and solvent engineering.[9,10,13−15] In conventional PSCs, the photo-absorber is sandwiched between the electron transport layer (ETL) and hole transport layer (HTL), where TiO_2 typically is employed as an ETL; however, the high temperature processing for its crystallization and sintering could increase the overall production cost and hence the commercialization.[16,17] To overcome this issue, an inverted p-i-n PSC structure has been developed and under extensive research, where organic ETLs such as PCBM are exploited, help in minimizing the density of defects in the perovskite/ETL interface, deliver a well-matched alignment of band structures, and so on.[18−21] Nevertheless, PSCs without ETL generally face substantial reduction in V_{oc}, J_{sc}, and FF and affect the overall device performance.[22−24] It is worth mentioning that the morphology of ETL and interactions between multiple interfaces within the device are very crucial for efficient charge transport and collection processes;[20,25,26] however, focused investigations on ETL morphology studies in PSCs are limited. There are few systematic studies that have been pursued on different mono-solvent systems followed with the prolonged solvent annealing process of ETL for complete evaporation of

Received: September 18, 2021
Accepted: December 13, 2021

the solvent and better perovskite/ETL interfacing, resulting in controlled film quality with respectable efficiency.[25,27,28] Liu and Lee[12] investigated the effect of 1,8-diiodooctane (DIO) as a solvent additive to control the PCBM-ETL morphology with an annealing temperature of 40 °C for 30 min in an inverted PSC architecture, achieving a PCE of 14.8%. Their results suggested that DIO as a solvent additive improves PCBM morphology and helps in better charge transportation. The same research group in 2018[29] studied the effect of various organic solvents including chlorobenzene, dichlorobenzene, and chloroform for preparing PCBM-ETL for inverted PSCs using the same parameters of annealing temperature and time (40 °C for 30 min) for PCBM drying. This investigation revealed that conductivity and ETL roughness depend on the solvent evaporation rate, and the dichlorobenzene processed PCBM showed better morphology with an enhanced PCE of 17.9%. Tsai et al.[30] also studied the effect of various processing solvents such as methylbenzene, chloroform, chlorobenzene, and dichlorobenzene on the morphology of PCBM-ETL and inverted PSC device efficiency enhancement. Greener solvents such as tetraethyl orthocarbonate for perovskite layer and anisole for PCBM processing (annealing temperature of 90 °C for 30 min) were introduced by replacing chlorobenzene, which resulted in better film morphology/charge transportations in PCSs with PCE enhancement to 18.1%.[31] To control the morphology of PCBM-ETL, the concept of doping PCBM was also investigated; it was found that poly(9,9-dioctylfluorene-co-benzothiadiazole) as a dopant in PCBM improves the film morphology and reduces surface roughness, which led to PCE enhancement from 12.6 to 15% in inverted PSCs.[32] Very recently, Li and co-workers[33] introduced poly(ethylene-covinylacetate) (EVA) as a solution additive in PCBM; the study showed that strong coupling between PCBM and EVA endorses better molecular stacking and hence improves the morphology and moisture stability, with an enhanced PCE of 19.3% in PSCs. A detailed investigation on perovskite-PCBM bulk heterojunction was conducted by Ha and co-workers[34] in planar PSCs, with PCE enhancement from 11 to 18% achieved by improving charge properties and perovskite film quality. Ha et al.[35] introduced an efficient strategy to control perovskite grain size by adding solubility dependent PCBM (annealing temperature of 110 °C for 10 min) in perovskite antisolvent and reported a PEC enhancement to 15.9% for the optimized PSCs.

The complexity in fabricating high-quality and uniform PCBM-ETL may cause severe non-radiation recombination at the perovskite/PCBM interface. Involvement of low boiling point anti-solvents generally leads to fast evaporation that tends to damage ETL morphology, which suffers from poor surface coverage and lack of interfacial contact between perovskite and ETL.[21,30,35,36]

To overcome the prolonged solvent annealing process, our mixed solvent strategy seems to be a highly beneficial and quick strategy to get a smooth film with reduced pinholes and better interface. However, in the present study, the ratio of the $CB_{0.5}$−$DCB_{0.5}$ mixed solvent strategy with variable boiling points and vapor pressures has been adjusted appropriately to get a uniform film with reduced pinholes on the PCBM surface to improve coverage and enhance PCBM film quality. This not only helps in fabricating a uniform ETL with improved morphology and provides better surface coverage but is also beneficial to execute the penetration of PCBM that helps in repairing the voids within the perovskite film and reinforce the interfacial contact in perovskite/ETL. The mixed solvent strategy here seems to be a highly beneficial and comparatively quick strategy to get a smooth film with reduced pinholes and better interface. The solvent engineering strategy here utilizes CB (low bp ∼131 °C) and DCB (high bp ∼180.5 °C) solvent systems, where DCB aids to slow evaporation with a lower vapor pressure of 0.16 kPa. The uniformity and better film quality of ETL were investigated using field emission scanning electron microscopy (FE-SEM) and atomic force microscopy (AFM). The steady-state results revealed strong quenching that is attributed to better charge extraction and strong interfacial contact in the perovskite/ETL interface with solvent engineering, i.e., $CB_{0.5}$−$DCB_{0.5}$ solvent system; furthermore, the findings were supported with the decay dynamics measured through TR-PL. The PCE in inverted planar PSCs increased from 17.2% for $CB_{1.0}$−DCB to 18.46% for $CB_{0.5}$−$DCB_{0.5}$ mixed solvent treated ETL, with minimum charge carrier recombination at the interface confirmed through the EIS study.

RESULTS AND DISCUSSION

The focus of the present study lies in the regime of solvent engineering and the effect of solvent optimization on the electron transport layer (ETL) and fabricating high-quality perovskite/ETL film without involving excess surface passivation and so on, which has been further used in inverted PSCs. To reveal the effectiveness of solvent engineering on ETL (PCBM) for uniform film quality and better interfacial contact of perovskite/ETL, we first conducted structural and optical characterizations on perovskite/ETL on glass substrates. Figure S1 (black line) displays the XRD pattern of pristine perovskite in the present study; the optimized perovskite composition, i.e., $BA_{0.02}(FA_{0.83}Cs_{0.17})_{0.98}Pb(I_{0.83}Br_{0.17})_3$, has been used throughout the experimental and device testing for all the cases. It has been revealed that the XRD observed here is phase pure for perovskite confirmed with the reference reported elsewhere[37] with an average grain size of 150 to 230 nm. In addition. The FE-SEM micrograph in Figure S2 depicts the morphology, grain size, and film coverage of the perovskite film. This was followed by the fabrication of PCBM (ETL) on top of the perovskite, where single and mixed solvent system of CB and DCB has been used as organic solvent for PCBM film casting on perovskite, i.e., $CB_{1.0}$−DCB_0 (1:0 v/v%), $CB_{0.75}$−$DCB_{0.25}$ (3:1 v/v%), $CB_{0.5}$−$DCB_{0.5}$ (1:1 v/v%), and CB_0−$DCB_{1.0}$ (0:1 v/v%). The vapor pressure and boiling point of the solvent for this experiment are shown in Table S1. Figure S1 depicts the X-ray diffraction of perovskite/ETL films for all the four cases, which confirmed the fabrication of pure phase perovskite without any impurity or degradation.[37] We have further conducted the in-plane GIXRD on $CB_{1.0}$−DCB_0 and $CB_{0.5}$−$DCB_{0.5}$ mono and mixed solvent treated PCBM ETL on the perovskite film, shown in Figure S3. As reported in the previous studies, PCBM helps in enhancing the crystallinity of halide perovskites;[38−40] the major peaks as observed correlate to the crystalline phase of the $BA_{0.02}(FA_{0.83}Cs_{0.17})_{0.98}Pb(I_{0.83}Br_{0.17})_3$ perovskite. However, it can be clearly observed that the perovskite crystallinity increased for the $CB_{0.5}$−$DCB_{0.5}$ mixed solvent treated PCBM as compared to the $CB_{1.0}$−DCB_0. Since the concentration of PCBM is constant in all the cases, the optimized ratio of solvents with different boiling points and vapor pressures of the mixed solvent system tends to slow the evaporation rate of the solvent and can control the

https://doi.org/10.1021/acsaem.1c02913
ACS Appl. Energy Mater. XXXX, XXX, XXX−XXX

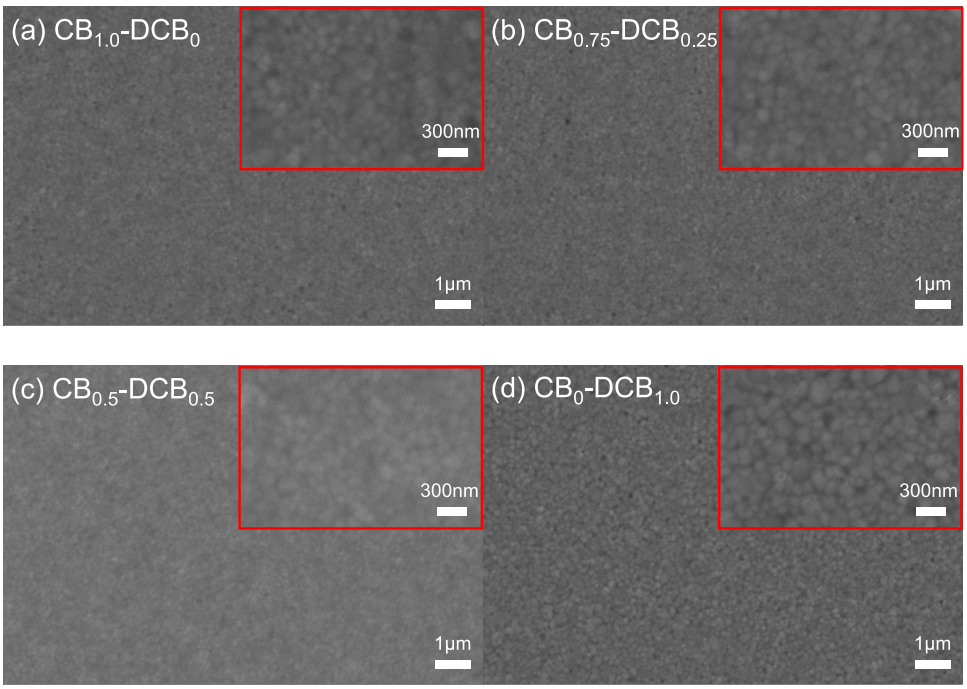

Figure 1. FE-SEM micrographs of solvent treated PCBM ETL in perovskite/PCBM films at 20k and 50k magnifications (inset): (a) $CB_{1.0}$–DCB_0, (b) $CB_{0.75}$–$DCB_{0.25}$, (c) $CB_{0.5}$–$DCB_{0.5}$, and (d) CB_0–$DCB_{1.0}$, respectively.

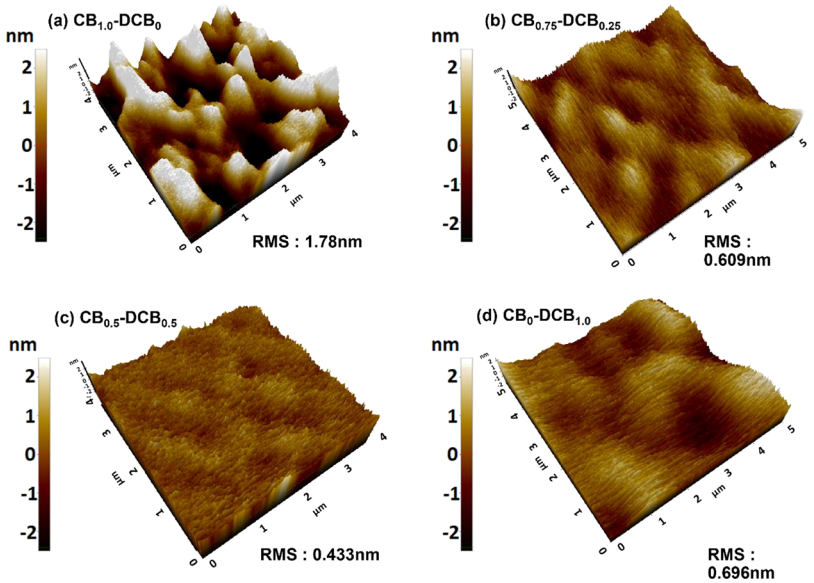

Figure 2. AFM micrographs of single and mixed solvent processed PCBM ETL in perovskite/PCBM films: (a) $CB_{1.0}$–DCB_0, (b) $CB_{0.75}$–$DCB_{0.25}$, (c) $CB_{0.5}$–$DCB_{0.5}$, and (d) CB_0–$DCB_{1.0}$.

morphology, provide uniformity, and reduce surface roughness.

Additionally, the morphological investigation and film coverage were conducted using FE-SEM and AFM measurements. Figure 1 shows FE-SEM micrographs of perovskite/PCBM surfaces for various solvent engineering cases.

Figure 1a,d demonstrates the perovskite/PCBM where chlorobenzene (CB) and dichlorobenzene (DCB) solvents were used as ETL solvent, respectively, and Figure 1b depicts the perovskite/PCBM where a mixed solvent ratio of $CB_{0.75}$–$DCB_{0.25}$ was used for ETL film casting on top of perovskite. It has been observed from FESEM micrographs that the film morphology is nonuniform and with pinholes, resulting in reduced film quality. However, in the mixed solvent case, i.e., $CB_{0.5}$–$DCB_{0.5}$ (Figure 1c), where an equal volume ratio of both solvents was used, better surface coverage and uniformity can be clearly seen. The solvent boiling point and vapor pressure play a vital role for achieving good quality film,[30] and in the present work, we have demonstrated that the optimized ratio of solvents with two different boiling points for ETL fabrication may result in better quality film. If the solvent boiling point is too low with high vapor pressure, it results in rapid drying of the film.[41] The solvent gets volatile during the spin coating process before the film gets evenly spread, resulting in reduced coverage and poor morphology,[30,42,43] as can be seen in $CB_{1.0}$–DCB_0 processed PCBM. In addition, we

https://doi.org/10.1021/acsaem.1c02913
ACS Appl. Energy Mater. XXXX, XXX, XXX−XXX

have observed pinholes and nonuniformity in the ETL film processed with 100% DCB solvent (CB_0–$DCB_{1.0}$), which might be due to insufficient annealing duration or temperature processing. The solvent annealing time and temperature are optimized as per the mixed solvent system; however, it seems inadequate for the single solvent processed PCBM. It can be clearly observed from Figure 2d that the film quality of CB_0–$DCB_{1.0}$ is almost the same as for the $CB_{1.0}$–DCB_0 processed ETL.

Figure 2 depicts the AFM micrographs of the perovskite/PCBM layer with single and mixed solvent systems for PCBM coating. The surface roughness values obtained were 1.78, 0.609, 0.433, and 0.696 nm for $CB_{1.0}$–DCB_0, $CB_{0.75}$–$DCB_{0.25}$, $CB_{0.5}$–$DCB_{0.5}$, and CB_0–$DCB_{1.0}$ solvent systems. The initial surface roughness of 1.78 nm was observed for the $CB_{1.0}$–DCB_0 case, which was reduced to 0.609 nm when 25% of CB was replaced with high bp solvent DCB and further reduced to 0.433 nm when the ratio of DCB was increased to 50% in the mixed solvent system, i.e., $CB_{0.5}$–$DCB_{0.5}$ for PCBM coating. The high value of surface roughness is attributed to the rapid volatilization of the solvent with lower bp (as listed in Table S1) that resulted in insufficient surface coverage in the case of $CB_{1.0}$–DCB_0 (depicted in Figure 2a). In addition, the surface roughness for CB_0–$DCB_{1.0}$ is higher than that of the mixed solvent processed PCBM films. In the present study, the ETL solvent annealing temperature is fixed to 120 °C for a duration of 10 min for quick annealing, which seems to be the optimized time period for mixed solvent processed PCBM films, where the presence of DCB retarded the rate of solvent evaporation and resulted in reduced surface roughness (shown in Figure 2b,c) and pinholes. The optimized ratio of high bp solvent in the mixed solvent system mitigates the degree of solvent volatilization and eases the formation of smooth and better quality films with reduced surface roughness by allowing the penetration of PCBM into perovskite voids.[25,44,45] However, for the CB_0–$DCB_{1.0}$ processed ETL layer, the solvent annealing time of 10 min for elevated temperature of 120 °C is inadequate; additionally, some traces of solvent may leave within the interface owing to its lower vapor pressure and result in the formation of surface defects.[46] However, the surface roughness of CB_0–$DCB_{1.0}$ is lower than that of $CB_{1.0}$–DCB_0 since the dielectric constant value of DCB (9.93) is higher than that of CB (5.62), which resembles the higher degree of solubility,[30] and hence the ETL processed with DCB is smoother with reduced surface roughness than CB processed ETL.

The above results indicate that the fabrication of a high-quality electron transport layer can be achieved by simply optimizing the solvent ratios in mixed solvent systems. The optimized ratio of the high bp solvent may control the growth rate with slow evaporation of solvent and allow the penetration of PCBM that helps in repairing the voids in perovskite, which helps in better crystallization of perovskite with reduced surface roughness and strengthens the coupling between perovskite and PCBM that will be discussed in detail in succeeding sections.

Figure 3a depicts the absorbance spectra of perovskite and perovskite/PCBM on glass substrates in the spectral range from 400 to 900 nm, and the calculated bandgap (1.64 eV) using the Tauc plot is provided in Figure S4. As denoted earlier, the various ratios of CB-DCB indicate the solvent optimization for PCBM layer fabrication on top of the perovskite layer. The light absorption intensities are almost

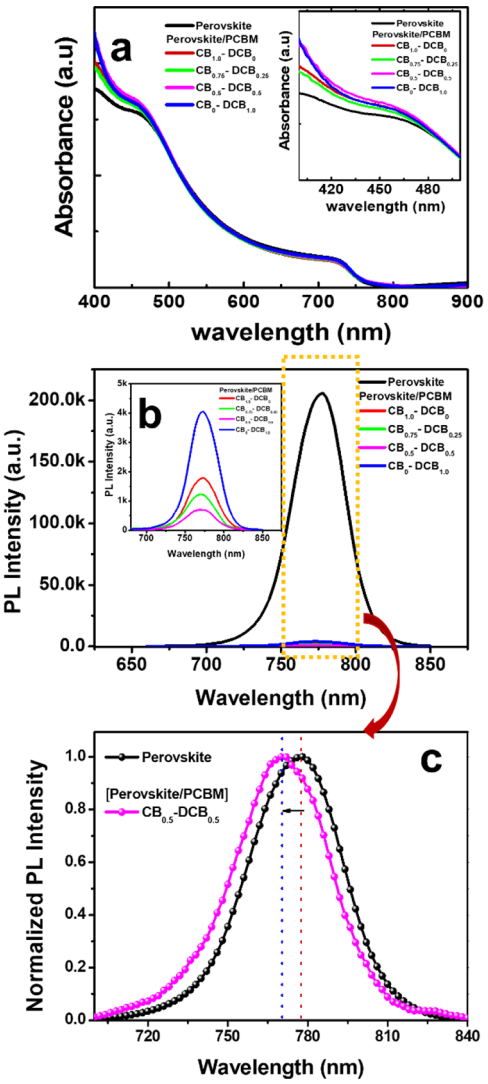

Figure 3. (a) UV–vis absorption spectra in the wavelength range of 400 to 900 nm; inset plot shows the magnified view in the range from 400 to 500 nm. (b) Steady-state PL spectra of perovskite film (black line) and perovskite/ETL films. PCBM electron transport layer treated with CB ($CB_{1.0}$–DCB_0, red curve), DCB (CB_0–$DCB_{1.0}$, blue curve), and mixed solvent systems $CB_{0.75}$–$DCB_{0.25}$ and $CB_{0.5}$–$DCB_{0.5}$ on glass substrate. (c) Normalized PL spectra of perovskite and perovskite/PCBM $CB_{0.5}$–$DCB_{0.5}$ indicating blue shift in PL spectra for perovskite/PCBM.

the same in the range of 480–650 nm; however, in the band range of 400–460 nm, the absorbance intensity increased after the deposition of PCBM on the perovskite layer. As shown in the inset of Figure 3a, a slight increase in the absorption for $CB_{1.0}$–DCB_0 was observed as compared to the $CB_{0.75}$–$DCB_{0.25}$ treated perovskite/PCBM film; in addition, the XRD peak intensity of the (100) and (110) hkl plane (Figure S1b) seems to be slightly increased for $CB_{1.0}$–DCB_0 as compared to $CB_{0.75}$–$DCB_{0.25}$. The increase in absorption might be attributed to the increased grain size and crystallinity of perovskite.[47] However, as discussed in the earlier section, the surface roughness for $CB_{1.0}$–DCB_0 was higher, which is ascribed to the rapid volatilization of the lower boiling point solvent that caused an insufficient surface coverage in case of $CB_{1.0}$–DCB_0. PCBM layers fabricated by the $CB_{0.5}$–$DCB_{0.5}$ solvent were observed to have a high light absorption

https://doi.org/10.1021/acsaem.1c02913
ACS Appl. Energy Mater. XXXX, XXX, XXX–XXX

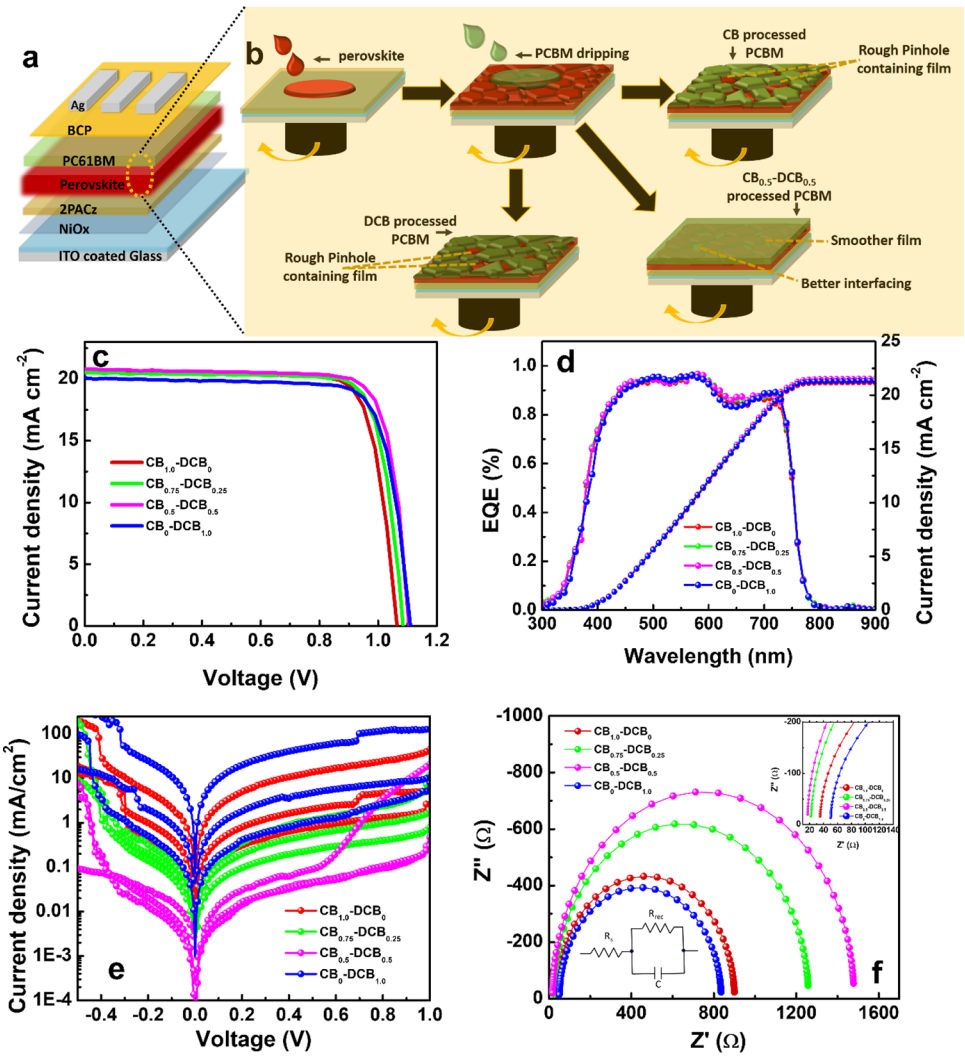

Figure 4. (a) Schematic for inverted PSC with the $BA_{0.02}(FA_{0.83}Cs_{0.17})_{0.98}Pb(I_{0.83}Br_{0.17})_3$ perovskite as photoabsorber. (b) Graphical representation of PCBM film processing with single and mixed solvent systems and their effect on the morphology and interface. (c) Current density−voltage (J−V) plots. (d) EQE spectra of the device to the different solvents in PCBM. (e) Dark current density−voltage plots for the three sets of devices in each case of single and mixed solvent processed PCBM ET layer in perovskite/PCBM films in inverted PSCs, i.e., $CB_{1.0}$−DCB_0 (red line), $CB_{0.75}$−$DCB_{0.25}$ (green line), $CB_{0.5}$−$DCB_{0.5}$ (magenta line), and CB_0−$DCB_{1.0}$ (blue line). (f) Impedance spectrum characterization; Nyquist plots of impedance spectra in PCBM layers manufactured from different PCBM solvents obtained by applying 1 V bias in the dark; fitting done with the equivalent circuit shown in panel f.

compared to other samples (as shown in the inset of Figure 3a), which might be attributed to the better film quality with reduced surface roughness and enhanced crystallinity of perovskite/PCBM $CB_{0.5}$−$DCB_{0.5}$,[47,48] which further supported the results obtained through AFM (Figure 2) and GIXRD data (Figure S3).

The mixed solvent strategy of using high boiling point solvents for ETL fabrication helps in the penetration of the ET organic molecule into the perovskite film below, which tends to develop a pseudo-bulk heterojunction and repair the defects of perovskite film,[25] further evidenced through PL results. Figure 3b illustrates the steady-state PL spectra of the pristine perovskite film and perovskite/ETL with various ratios of the mixed CB−DCB solvent system. Steady-state PL quenching has been realized in perovskite/PCBM-ETL, which indicates the charge transport.[49−52] Since the interaction between perovskite/PCBM leads to the charge extraction process from perovskite to PCBM, several pioneering works have already been done on the charge extraction from perovskite to ETL/HTL and quenching in PL intensity.[38,53−55] In the case of the $CB_{0.5}$−$DCB_{0.5}$ solvent treated PCBM film, the quenching is comparatively higher, which may be attributed to the better charge transport. However, when considering the layer stacking of perovskite with ETL/HTL or even the complete device, the concept of photoluminescence quenching in SS-PL cannot be merely considered due to the charge transfer from perovskite to the extraction layer, though it also includes other physical effects such as charge carrier recombinations and trapping within the layer and at the perovskite−ETL interface.[54,56] As we have discussed in earlier sections, where the surface morphology was hampered in the case of the CB_0−$DCB_{1.0}$ solvent processed PCBM and resulted in a nonuniform film with comparatively higher surface roughness than mixed cases, this might be due to the inadequate duration of solvent annealing in the case of the solvent with lower vapor pressure, which might result in the surface defects. Hence, PL quenching in $CB_{0.5}$−$DCB_{0.5}$ treated ETL in perovskite/ETL specifies the better charge transport in

https://doi.org/10.1021/acsaem.1c02913
ACS Appl. Energy Mater. XXXX, XXX, XXX−XXX

Table 1. PV Parameters of Mixed Solvent Processed PCBM ETL in Perovskite/PCBM Films for Inverted PSCs under AM 1.5 Illumination

perovskite		J_{sc} (mA cm^{-2})	V_{oc} (V)	FF (%)	PCE (%)
$CB_{1.0}$–DCB_0	average	19.62±0.38	1.077±0.01	79.8±0.68	16.89±0.35
	champion	20.18	1.099	79.18	17.72
$CB_{0.75}$–$DCB_{0.25}$	average	20.02±0.44	1.07±0.02	80.50±0.76	17.24±0.42
	champion	20.44	1.092	79.61	17.77
$CB_{0.5}$–$DCB_{0.5}$	average	20.2±0.5	1.092±0.01	80.93±0.9	17.86±0.36
	champion	20.81	1.106	80.21	18.46
CB_0–$DCB_{1.0}$	average	19.93±0.6	1.086±0.02	77.84±1.75	16.84±0.54
	champion	20.01	1.11	79.1	17.57

the perovskite/ETL interface. Steady-state (SS) PL measurements were further conducted with perovskite and perovskite/PCBM films over a range of time for each case. There is only a slight variation in PL intensity that has been observed in the SS-PL data over time from 0 to 5 min specially after 5 min PL data, as shown in Figure S5a–e along with the statistical data on time vs PL intensity (Figure S5f). The measurements were all performed at the top surface of the film in perovskite/PCBM, and there was a prominent blue shift of approx. 6 nm detected for the perovskite/PCBM bilayer (771 nm) shown in Figure 3c and Figure S5, which might be attributed to the passivation of trap states. It has already been reported elsewhere that the SS-PL wavelength shifts toward the blue region for the perovskite/PCBM bilayer, which might be ascribed to trap state passivation on the top surface or near grain boundaries.[38,57] In the present investigation, we have observed that the optimized concentration of the high boiling point solvent in the mixed solvent system lessens the solvent volatilization and helps in the fabrication of a smooth and better quality film with reduced surface roughness (as depicted in the GIXRD and AFM data) by allowing the penetration of PCBM into the voids in the perovskite film. Based on these observations, we can correlate the development of better quality film formation with reduced traps at the surface and grain boundaries and hence its effect on the optical property of perovskite. To check the consistency in PL intensity throughout the film, SS-PL measurements at three different points within the same film in selected pristine perovskite and perovskite/PCBM ($CB_{0.5}$–$DCB_{0.5}$) film (as shown in Figure S6) were further conducted with constant instrumental parameters. The inset in Figure S6 (right panel) shows the SS-PL graph for perovskite/PCBM ($CB_{0.5}$–$DCB_{0.5}$) film with almost equal intensities at different spot points, and Figure S6 (left panel) shows the histogram for both sample intensities at three different points that confirms the consistency in PL intensities.

TRPL measurement was further conducted for perovskite and perovskite/PCBM on glass substrate to elucidate the evidenced quenching in steady-state PL spectra to realize the effect of mixed solvent treatment on perovskite/PCBM charge transfer.

The average lifetime was calculated with the formula $\tau_{avg} = \sum \alpha_i \tau_i^2 / \sum \alpha_i \tau_i$.[58] A reduction in average lifetime was observed from 23.2 ns (perovskite) to 2.35 ns (Figure S7 and Table S2) for the $CB_{0.5}$–$DCB_{0.5}$ mixed solution-treated PCBM ETL in perovskite/PCBM film. The results obtained for the $CB_{0.5}$–$DCB_{0.5}$ case shows better charge extraction[33,54,59] as compared to the other films. In other words, the $CB_{0.5}$–$DCB_{0.5}$ mixed solution-treated PCBM ETL in perovskite/ETL film allows efficient charge transfer to the contact layer resulting in a shorter PL lifetime.

To elucidate the effect of solvent on the PCBM layer on the device performance, the PSCs glass/ITO/NiOx/2PACz/$BA_{0.02}(FA_{0.83}Cs_{0.17})_{0.98}Pb(I_{0.83}Br_{0.17})_3$/PCBM/BCP/Ag were fabricated for the $CB_{1.0}$–DCB_0, $CB_{0.75}$–$DCB_{0.25}$, $CB_{0.5}$–$DCB_{0.5}$, and CB_0–$DCB_{1.0}$ solvent processed PCBM layer in perovskite solar cells, and the device structure is shown in Figure 4a. Based on the above results and related explanations, the plausible schematic representation is depicted in Figure 4b. The solvent processing with mono and mixed solvent systems and their effect on the morphology of PCBM were studied with SEM and AFM results. Figure 4b shows the illustrative representation in which, for pure CB and DCB cases, the PCBM film is nonuniform with high surface roughness and pinholes, which are attributed to the fast solvent evaporation of the solvent in the former case and inadequate processing parameters for the latter one. Nevertheless, in case of the mixed solvent processed PCBM film, the surface coverage is comparatively better (as observed from SEM and AFM micrographs), and based on the significant increase in steady-state PL quenching and efficient charge extraction from TRPL data, it can be concluded that simply increasing the concentration of the solvent with lower vapor pressure up to an optimized ratio benefits the penetration of PCBM within the perovskite voids and helps in defect passivation, which may lead to enhanced interfacial interaction and better charge extraction and transport.[25,60]

The J–V characteristics and detailed photoelectric parameters of PSCs fabricated from different solvent processing of the PCBM in PSCs are shown in Figure 4c and Table 1. For $CB_{1.0}$–DCB_0, $CB_{0.75}$–$DCB_{0.25}$, $CB_{0.5}$–$DCB_{0.5}$, and CB_0–$DCB_{1.0}$ as solvents processed PCBM, the PCEs for champion devices are 17.72, 17.77, 18.46, and 17.57%, respectively, whereas Figure S8 depicts the statistical distribution of PCEs in 22 devices. In addition, Table S3 summarizes the best reported efficiencies in the literature of very similar mixed halide–mixed cation Pb-based perovskite solar absorbers and as reported in the present work.

With a champion device PCE of 18.46%, the stabilized power output (SPO) of 17.6% has been achieved as depicted in Figure S9. It has been observed that the value of current density (J_{sc}) is minimum for $CB_{1.0}$–DCB_0 (20.1 mA/cm^2) and CB_0–$DCB_{1.0}$ (20.01 mA/cm^2); however, with replacement of 25% CB with DCB in the $CB_{0.75}$–$DCB_{0.25}$ solvent treated PCBM layer, the J_{sc} increases to 20.44 mA/cm^2, and with further increase in the contribution of DCB to 50% in the mixed solvent treated PCBM ($CB_{0.5}$–$DCB_{0.5}$), the J_{sc} increases to 20.81 mA/cm^2.

https://doi.org/10.1021/acsaem.1c02913
ACS Appl. Energy Mater. XXXX, XXX, XXX–XXX

In addition, with the use of $CB_{0.5}$−$DCB_{0.5}$ as PCBM solvent, a very small increase in the average open circuit voltage (V_{oc} ~1.1 V) and fill factor (FF ~80.21) was observed, which can be considered to be due to improved film and charge extraction in perovskite/PCBM. Since the higher internal voltage relates to the open circuit voltage (V_{oc}) of the device, in-depth study on this relation have been reported in some pioneering research that the V_{oc} equals the internal voltage only for the high efficiency PSCs, whereas V_{oc} is lower than the internal voltage in case of poor efficiency devices.[61,62] However, in the present study, we have observed SS-PL intensity reduction that depends on various physical effects, which can be correlated to the V_{oc} as stated earlier. Nevertheless, the variation in the V_{oc} is within a small window to be justified with respect to the internal voltage, and exploring this insight and correlations is a subject of future investigation.

Figure 4d displays the external quantum efficiency (EQE) curves for $CB_{1.0}$−DCB_0, $CB_{0.75}$−$DCB_{0.25}$, $CB_{0.5}$−$DCB_{0.5}$, and CB_0−$DCB_{1.0}$ solvent processed PCBM. The PCBM with $CB_{0.5}$−$DCB_{0.5}$ system showed the highest EQE value in the wavelength range of 630 to 700 nm. This has been attributed to better film quality with maximum surface coverage and enhanced interaction between perovskite and PCBM, which leads to improved light absorption and charge collection and more efficient charge separation.[63−65]

Figure 4e depicts the dark J−V curves for $CB_{1.0}$−DCB_0, $CB_{0.75}$−$DCB_{0.25}$, $CB_{0.5}$−$DCB_{0.5}$, and CB_0−$DCB_{1.0}$ solvent processed PCBM in PSCs. For the $CB_{0.5}$−$DCB_{0.5}$ solvent system processed PCBM in perovskite solar cells, the reverse bias is lower in comparison to the other three cases, suggesting that the PCBM has less leakage current for the $CB_{0.5}$−$DCB_{0.5}$ solvent processed PCBM in PSC. As discussed in the earlier sections, the morphology control and film uniformity play a vital role on the device performance, and it has been observed that the films fabricated with $CB_{1.0}$−DCB_0 and CB_0−$DCB_{1.0}$ have comparatively nonuniform surface, pinholes, and high surface roughness (as shown in FE-SEM and AFM micrographs, Figures 1 and 2). The leakage current reduction in dark J−V relates to the reduced trap densities that correlate to the crystallinity of the perovskite film and reduced non-radiative recombinations.[66] The dark J−V trend for $CB_{0.5}$−$DCB_{0.5}$ (magenta line) and $CB_{0.75}$−$DCB_{0.25}$ (green line) for all the three set of devices is consistent; however, as shown in Figure 4e, in $CB_{1.0}$−DCB_0 and CB_0−$DCB_{1.0}$, due to the existence of non-uniformity in film morphology, the dark J−V data show inconsistency.

Figure 4f shows the Nyquist plot obtained by applying 1 V bias in the dark for CB ($CB_{1.0}$−DCB_0), DCB (CB_0−$DCB_{1.0}$), and mixed solvent ($CB_{0.75}$−$DCB_{0.25}$ and $CB_{0.5}$−$DCB_{0.5}$) processed PCBM electron transport layer for PSCs. The semicircle in Figure 4f provides information about the charge recombination resistance (R_{rec}). As shown in Table S4, the values obtained from the impedance study for the series show the same trend observed in J−V parameters for all the cases. The Rs value reduced from 32.5 to 16.9 Ω for $CB_{1.0}$−DCB_0 and $CB_{0.5}$−$DCB_{0.5}$, respectively. This result is consistent with the series resistance reduction for $CB_{0.5}$−$DCB_{0.5}$ determined from the J−V curve. Moreover, the factors affecting device fill factor are generally the impedance between perovskite/ETL, series (Rs), and shunt resistance (Rsh). The Rs for $CB_{0.5}$−$DCB_{0.5}$ treated PCBM layer in PSCs is much lower at approx. 16.9 Ω, and by keenly correlating this with the AFM surface roughness where the surface roughness was minimum for the case of $CB_{0.5}$−$DCB_{0.5}$, it can be concluded that the ETL surface was smoother and the resistance between perovskite/ETL decreased when 50% of low bp solvent was replaced by high bp DCB for processing PCBM layer in PSCs, which is attributed to the enhanced FF, interfacial coupling, and charge dissociation. In addition, the R_{rec} value is the highest (R_{rec} = 1461.94 Ω) for $CB_{0.5}$−$DCB_{0.5}$ as a solvent for PCBM in PSC, which can help in improving the perovskite/PCBM interface by allowing slow evaporation of the solvent and easing the diffusion of PCBM into perovskite voids, which helps in repairing the perovskite surface, eventually strengthening the interfacial interaction between perovskite and PCBM, preventing electron−hole recombination, and improving electron transport.[67,68] However, in case of CB_0−$DCB_{1.0}$ where the 100% DCB was used to process the PCBM layer, due to the higher boiling point and too low vapor pressure, the solvent evaporation becomes slower, which may result in the formation of surface defects, which can be clearly observed with the increased value of series resistance. The mixed solvent processing of the PCBM layer helps in the fabrication of smoother ETL with maximum surface coverage. Eventually, the existence of high boiling point DCB solvent in the optimum concentration leads to the slow evaporation of the solvent and penetration of PCBM within perovskite holes, resulting in improved interfacial coupling and hence better charge extraction and device performance. Therefore, this study provides a way to improve the device performance of PSCs by employing a simple mixed solvent strategy for electron transport layer processing.

CONCLUSIONS

High-quality PCBM-ETL film fabrication for inverted PSC has been achieved through a mixed solvent engineering strategy using CB and DCB solvents. It has been shown to cause strong interfacial coupling between perovskite and ETL, which significantly results in strong PL quenching in mixed solvent treated ETL, further confirmed with the decay dynamics. Moreover, the variation of boiling points in this mixed solvent system leads to the slow evaporation of the solvent, controls the rate of ETL drying, and helps the PCBM to patch the voids and non-uniform surfaces in the perovskite film. TR-PL and EIS measurements revealed lesser electron−hole recombination at the perovskite/ETL interface, thus improving the electron collection efficiency. The PSC results revealed an efficient enhancement in the device performance of 18.46%. Our finding provides an in-depth understanding of how the mixed solvent systems promote better film fabrication of PCBM-ETL by precisely modifying the solvent ratio in the mixed solvent system and helps in enhancing the interfacial contact of perovskite/ETL without involving extra surface passivation, which further aids in the efficient charge extraction and hence helps in increasing the device performance in PSCs.

ASSOCIATED CONTENT

Supporting Information

The Supporting Information is available free of charge at https://pubs.acs.org/doi/10.1021/acsaem.1c02913.

Experimental and measurement details: perovskite preparation method, perovskite solar cells fabrication, related characterization techniques; XRD of pristine and perovskite/PCBM; FESEM of pristine perovskite;

https://doi.org/10.1021/acsaem.1c02913
ACS Appl. Energy Mater. XXXX, XXX, XXX−XXX

statistical distribution of PCEs; and summarized boiling points of solvents, TRPL parameters, and EIS parameters in tabular form (PDF)

AUTHOR INFORMATION

Corresponding Author

Dong-Won Kang − *Department of Smart City and Department of Energy Systems Engineering, Chung-Ang University, Seoul 06974, Republic of Korea;* orcid.org/0000-0002-4818-8108; Email: kangdwn@cau.ac.kr

Authors

SungWon Cho − *Department of Smart City, Chung-Ang University, Seoul 06974, Republic of Korea*

Padmini Pandey − *Department of Energy Systems Engineering, Chung-Ang University, Seoul 06974, Republic of Korea*

Jinwoo Park − *Department of Materials Science and Engineering, Seoul National University, Seoul 08826, Republic of Korea*

Tae-Woo Lee − *Department of Materials Science and Engineering, Seoul National University, Seoul 08826, Republic of Korea; Institute of Engineering Research, Nano System Institute (NSI), BK21 PLUS SNU Materials Division for Educating Creative Global Leaders, School of Chemical and Biological Engineering, Seoul National University, Seoul 08826, Republic of Korea*

Complete contact information is available at: https://pubs.acs.org/10.1021/acsaem.1c02913

Notes

The authors declare no competing financial interest.

ACKNOWLEDGMENTS

This work was supported by the National Research Foundation of Korea (NRF) grant funded by the Korea government (MSIT) (NRF 2021R1A2C4002045, 2021R1A4A2001687, and 2021K2A9A2A08000082).

REFERENCES

(1) Lanzetta, L.; Aristidou, N.; Haque, S. A. Stability of Lead and Tin Halide Perovskites: The Link between Defects and Degradation. *J. Phys. Chem. Lett.* **2020**, *11*, 574−585.

(2) Krishnamurthy, S.; Pandey, P.; Kaur, J.; Chakraborty, S.; Nayak, P.; Sadhanala, A.; Ogale, S. B. Organic-Inorganic Hybrid and Inorganic Halide Perovskites: Structural and Chemical Engineering, Interfaces and Optoelectronic Properties. *J. Phys. D: Appl. Phys.* **2020**, *54*, 133002.

(3) Ball, J. M.; Petrozza, A. Defects in Perovskite-Halides and Their Effects in Solar Cells. *Nat. Energy* **2016**, *1*, 1−13.

(4) Jeong, J.; Kim, M.; Seo, J.; Lu, H.; Ahlawat, P.; Mishra, A.; Yang, Y.; Hope, M. A.; Eickemeyer, F. T.; Kim, M.; Yoon, Y. J.; Choi, I. W.; Darwich, B. P.; Choi, S. J.; Jo, Y.; Lee, J. H.; Walker, B.; Zakeeruddin, S. M.; Emsley, L.; Rothlisberger, U.; Hagfeldt, A.; Kim, D. S.; Grätzel, M.; Kim, J. Y. Pseudo-Halide Anion Engineering for α-FAPbI 3 Perovskite Solar Cells. *Nature* **2021**, *592*, 381−385.

(5) Wang, R.; Huang, T.; Xue, J.; Tong, J.; Zhu, K.; Yang, Y. Prospects for Metal Halide Perovskite-based Tandem Solar Cells. *Nat. Photonics* **2021**, *15*, 411−425.

(6) Chen, P.; Bai, Y.; Wang, L. Minimizing Voltage Losses in Perovskite Solar Cells. *Small Struct.* **2021**, *2*, 2000050.

(7) Ünlü, F.; Jung, E.; Haddad, J.; Kulkarni, A.; Öz, S.; Choi, H.; Fischer, T.; Chakraborty, S.; Kirchartz, T.; Mathur, S. Understanding the Interplay of Stability and Efficiency in A-site Engineered Lead Halide Perovskites. *APL Mater.* **2020**, *8*, No. 070901.

(8) Choi, H.; Choi, K.; Choi, Y.; Kim, T.; Lim, S.; Park, T. A Review on Reducing Grain Boundaries and Morphological Improvement of Perovskite Solar Cells from Methodology and Material-Based Perspectives. *Small Methods* **2020**, *4*, 1900569.

(9) Lan, C.; Lan, H.; Liang, G.; Zhao, J.; Peng, H.; Fan, B.; Zheng, Z.; Sun, H.; Luo, J.; Fan, P.; Fu, Y. Q. Simultaneous Formation of CH3NH3PbI3 and Electron Transport Layers using Antisolvent Method for Efficient Perovskite Solar Cells. *Thin Solid Films* **2018**, *660*, 75−81.

(10) Yang, L.; Gao, Y.; Wu, Y.; Xue, X.; Wang, F.; Sui, Y.; Sun, Y.; Wei, M.; Liu, X.; Liu, H. Novel Insight into the Role of Chlorobenzene Antisolvent Engineering for Highly Efficient Perovskite Solar Cells: Gradient Diluted Chlorine Doping. *ACS Appl. Mater. Interfaces* **2019**, *11*, 792−801.

(11) Liu, X.; Xu, C.; Lee, E.-C. Chlorobenzene-Mediated Control of Crystallization in Perovskite Films for High-Performance Solar Cells. *ACS Appl. Energy Mater.* **2020**, *3*, 12291−12297.

(12) Liu, Z.; Lee, E.-C. Solvent Engineering of the Electron Transport Layer using 1, 8-Diiodooctane for Improving the Performance of Perovskite Solar Cells. *Org. Electron.* **2015**, *24*, 101−105.

(13) Yi, A.; Chae, S.; Lee, H.; Kim, H. J. The Synergistic Effect of Cooperating Solvent Vapor Annealing for High-Efficiency Planar Inverted Perovskite Solar Cells. *J. Mater. Chem. A* **2019**, *7*, 27267−27277.

(14) Jang, G.; Ma, S.; Kwon, H.-C.; Goh, S.; Ban, H.; Lee, J.; Lee, C. U.; Moon, J. Binary Antisolvent Bathing Enabled Highly Efficient and Uniform Large-area Perovskite Solar Cells. *Chem. Eng. J.* **2021**, *423*, 130078.

(15) Bing, J.; Huang, S.; Ho-Baillie, A. W. Y. A Review on Halide Perovskite Film Formation by Sequential Solution Processing for Solar Cell Applications. *Energy Technol.* **2020**, *8*, 1901114.

(16) Tao, C.; Neutzner, S.; Colella, L.; Marras, S.; Kandada, A. R. S.; Gandini, M.; De Bastiani, M.; Pace, G.; Manna, L.; Caironi, M.; Bertarelli, C. 17.6% Stabilized Efficiency in Low-temperature processed Planar Perovskite Solar Cells. *Energy Environ. Sci.* **2015**, *8*, 2365−2370.

(17) Kim, B. J.; Kim, D. H.; Lee, Y.-Y.; Shin, H.-W.; Han, G. S.; Hong, J. S.; Mahmood, K.; Ahn, T. K.; Joo, Y.-C.; Hong, K. S.; Park, N. G.; Lee, S.; Jung, H. S. Highly Efficient and Bending Durable Perovskite Solar Cells: Toward a Wearable Power Source. *Energy Environ. Sci.* **2015**, *8*, 916−921.

(18) Wojciechowski, K.; Leijtens, T.; Siprova, S.; Schlueter, C.; Hörantner, M. T.; Wang, J. T.-W.; Li, C.-Z.; Jen, A. K.-Y.; Lee, T.-L.; Snaith, H. J. C60 as an Efficient n-type Compact Layer in Perovskite Solar Cells. *J. Phys. Chem. Lett.* **2015**, *6*, 2399−2405.

(19) Dong, S.; Wan, Y.; Wang, Y.; Yang, Y.; Wang, Y.; Zhang, X.; Cao, H.; Qin, W.; Yang, L.; Yao, C.; Ge, Z.; Yin, S. Polyethylenimine as a Dual Functional Additive for Electron Transporting Layer in Efficient Solution Processed Planar Heterojunction Perovskite Solar Cells. *RSC Adv.* **2016**, *6*, 57793−57798.

(20) Xia, F.; Wu, Q.; Zhou, P.; Li, Y.; Chen, X.; Liu, Q.; Zhu, J.; Dai, S.; Lu, Y.; Yang, S. Efficiency Enhancement of Inverted Structure Perovskite Solar Cells via Oleamide Doping of PCBM Electron Transport Layer. *ACS Appl. Mater. Interfaces* **2015**, *7*, 13659−13665.

(21) Elnaggar, M.; Elshobaki, M.; Mumyatov, A.; Luchkin, S. Y.; Dremova, N. N.; Stevenson, K. J.; Troshin, P. A. Molecular Engineering of the Fullerene-Based Electron Transport Layer Materials for Improving Ambient Stability of Perovskite Solar Cells. *Sol. RRL* **2019**, *3*, 1900223.

(22) Noh, M. F. M.; Teh, C. H.; Daik, R.; Lim, E. L.; Yap, C. C.; Ibrahim, M. A.; Ludin, N. A.; bin Mohd Yusoff, A. R.; Jang, J.; Teridi, M. A. M. The Architecture of the Electron Transport Layer for a Perovskite Solar Cell. *J. Mater. Chem. C* **2018**, *6*, 682−712.

(23) Zhang, Y.; Liu, M.; Eperon, G. E.; Leijtens, T. C.; McMeekin, D.; Saliba, M.; Zhang, W.; de Bastiani, M.; Petrozza, A.; Herz, L. M.; Johnston, M. B.; Lin, H.; Snaith, H. J. Charge Selective Contacts,

Mobile Ions and Anomalous Hysteresis in Organic−Inorganic Perovskite Solar Cells. *Mater. Horiz.* **2015**, *2*, 315−322.
(24) Ke, W.; Fang, G.; Wan, J.; Tao, H.; Liu, Q.; Xiong, L.; Qin, P.; Wang, J.; Lei, H.; Yang, G. Efficient Hole-Blocking Layer-Free Planar Halide Perovskite Thin-Film Solar Cells. *Nat. Commun.* **2015**, *6*, 1−7.
(25) Wu, C.-G.; Chiang, C.-H.; Chang, S. H. A Perovskite Cell with a Record-High-Voc of 1.61 V based on Solvent Annealed CH 3 NH 3 PbBr 3/ICBA Active Layer. *Nanoscale* **2016**, *8*, 4077−4085.
(26) Kim, T.; Lim, J.; Song, S. Recent Progress and Challenges of Electron Transport Layers in Organic−Inorganic Perovskite Solar Cells. *Energies* **2020**, *13*, 5572.
(27) Shao, Y.; Yuan, Y.; Huang, J. Correlation of Energy Disorder and Open-Circuit Voltage in Hybrid Perovskite Solar Cells. *Nat. Energy* **2016**, *1*, 1−6.
(28) Xiao, Z.; Dong, Q.; Bi, C.; Shao, Y.; Yuan, Y.; Huang, J. Solvent Annealing of Perovskite-Induced Crystal Growth for Photovoltaic-Device Efficiency Enhancement. *Adv. Mater.* **2014**, *26*, 6503−6509.
(29) Liu, Z.; Xie, X.; Lee, E.-C. Effects of Organic Solvents for the Phenyl-C61-Butyric Acid Methyl Ester Layer on the Performance of Inverted Perovskite Solar Cells. *Org. Electron.* **2018**, *56*, 247−253.
(30) Tsai, C.-H.; Lin, C.-M.; Kuei, C.-H. Investigation of the Effects of Various Organic Solvents on the PCBM Electron Transport Layer of Perovskite Solar Cells. *Coatings* **2020**, *10*, 237.
(31) Wang, M.; Fu, Q.; Yan, L.; Huang, J.; Ma, Q.; Humayun, M.; Pi, W.; Chen, X.; Zheng, Z.; Luo, W. Systematic Optimization of Perovskite Solar Cells via Green Solvent Systems. *Chem. Eng. J.* **2020**, *387*, 123966.
(32) Jiang, M.; Niu, Q.; Tang, X.; Zhang, H.; Xu, H.; Huang, W.; Yao, J.; Yan, B.; Xia, R. Improving the Performances of Perovskite Solar Cells via Modification of Electron Transport Layer. *Polymer* **2019**, *11*, 147.
(33) Li, J.; Meng, X.; Huang, Z.; Dai, R.; Sheng, W.; Gong, C.; Tan, L.; Chen, Y. A Regularity-Based Fullerene Interfacial Layer for Efficient and Stable Perovskite Solar Cells via Blade-Coating. *Adv. Funct. Mater.* **2021**, *2105917*, 2105917.
(34) Ha, S. R.; Jeong, W. H.; Liu, Y.; Oh, J. T.; Bae, S. Y.; Lee, S.; Kim, J. W.; Bandyopadhyay, S.; Jeong, H. I.; Kim, J. Y.; Kim, Y.; Song, M. H.; Park, S. H.; Stranks, S. D.; Lee, B. R.; Friend, R. H.; Choi, H. Molecular Aggregation Method for Perovskite−Fullerene Bulk Heterostructure Solar Cells. *J. Mater. Chem. A* **2020**, *8*, 1326−1334.
(35) Ha, S. R.; Yoon, S.; Eom, S.; Jeong, W. H.; Woo, J.; Yang, J.; Sung, D.; Oh, J. T.; Jeong, H. I.; Choi, W. I. Multi-Scalable Grain Growth via Phenyl-C60-Butyric Acid Methyl Ester Molecular Aggregation in Perovskite Solar Cells. *ACS Appl. Energy Mater.* **2021**, *6*, 5985−5994.
(36) Chang, C.-Y.; Huang, W.-K.; Chang, Y.-C.; Lee, K.-T.; Chen, C.-T. A Solution-Processed n-Doped Fullerene Cathode Interfacial Layer for Efficient and Stable Large-Area Perovskite Solar Cells. *J. Mater. Chem. A* **2016**, *4*, 640−648.
(37) Wang, Z.; Lin, Q.; Chmiel, F. P.; Sakai, N.; Herz, L. M.; Snaith, H. J. Efficient Ambient-Air-Stable Solar Cells with 2D−3D Heterostructured Butylammonium-Caesium-Formamidinium Lead Halide Perovskites. *Nat. Energy* **2017**, *2*, 17135.
(38) Park, C.; Ko, H.; Sin, D. H.; Song, K. C.; Cho, K. Organometal Halide Perovskite Solar Cells with Improved Thermal Stability via Grain Boundary Passivation using a Molecular Additive. *Adv. Funct. Mater.* **2017**, *27*, 1703546.
(39) Chiang, C.-H.; Wu, C.-G. Bulk Heterojunction Perovskite−PCBM Solar Cells with High Fill Factor. *Nat. Photonics* **2016**, *10*, 196−200.
(40) Zhong, Y.; Suzuki, K.; Inoue, D.; Hashizume, D.; Izawa, S.; Hashimoto, K.; Koganezawa, T.; Tajima, K. Interface-Induced Crystallization and Nanostructure Formation of [6, 6]-Phenyl-C 61-Butyric Acid Methyl Ester (PCBM) in Polymer Blend Films and its Application in Photovoltaics. *J. Mater. Chem. A* **2016**, *4*, 3335−3341.
(41) Noel, N. K.; Habisreutinger, S. N.; Wenger, B.; Klug, M. T.; Hörantner, M. T.; Johnston, M. B.; Nicholas, R. J.; Moore, D. T.; Snaith, H. J. A Low Viscosity, Low Boiling Point, Clean Solvent System for the Rapid Crystallisation of Highly Specular Perovskite Films. *Energy Environ. Sci.* **2017**, *10*, 145−152.
(42) Kim, Y. S.; Lee, Y.; Kim, J. K.; Seo, E.-O.; Lee, E.-W.; Lee, W.; Han, S.-H.; Lee, S.-H. Effect of Solvents on the Performance and Morphology of Polymer Photovoltaic Devices. *Curr. Appl. Phys.* **2010**, *10*, 985−989.
(43) Konstantakou, M.; Perganti, D.; Falaras, P.; Stergiopoulos, T. Anti-Solvent Crystallization Strategies for Highly Efficient Perovskite Solar Cells. *Crystals* **2017**, *7*, 291.
(44) Zhang, F.; Shi, W.; Luo, J.; Pellet, N.; Yi, C.; Li, X.; Zhao, X.; Dennis, T. J. S.; Li, X.; Wang, S.; Xiao, Y.; Zakeeruddin, S. M.; Bi, D.; Grätzel, M. Isomer-Pure Bis-PCBM-Assisted Crystal Engineering of Perovskite Solar Cells Showing Excellent Efficiency and Stability. *Adv. Mater.* **2017**, *29*, 1606806.
(45) Lin, X.; Cui, D.; Luo, X.; Zhang, C.; Han, Q.; Wang, Y.; Han, L. Efficiency Progress of Inverted Perovskite Solar Cells. *Energy Environ. Sci.* **2020**, *13*, 3823−3847.
(46) Lee, K.-M.; Chan, S.-H.; Chiu, W.-H.; Ahn, S.; Ting, C.-C.; Chang, Y.-H.; Suryanarayanan, V.; Wu, M.-C.; Liu, C.-Y. Reducing Defects in Organic-Lead Halide Perovskite Film by Delayed Thermal Annealing Combined with KI/I2 for Efficient Perovskite Solar Cells. *Nanomaterials* **2021**, *11*, 1607.
(47) Chen, Q.; Ke, J. C.-R.; Wang, D.; Mokhtar, M. Z.; Thomas, A. G.; Liu, Z. Impact of Halide Additives on Green Antisolvent and High-Humidity Processed Perovskite Solar Cells. *Appl. Surf. Sci.* **2021**, *536*, 147949.
(48) Hossain, M.; Arunagirinathan, R. N.; Garai, R.; Gupta, R. K.; Iyer, P. K. Enhancing the Efficiency and Ambient Stability of Perovskite Solar Cells via a Multifunctional Trap Passivation Molecule. *J. Mater. Chem. C* **2021**, *9*, 14309−14317.
(49) Wang, H.; Yang, F.; Li, N.; Kamarudin, M. A.; Qu, J.; Song, J.; Hayase, S.; Brabec, C. J. Efficient Surface Passivation and Electron Transport Enable Low Temperature-Processed Inverted Perovskite Solar Cells with Efficiency over 20%. *ACS Sustainable Chem. Eng.* **2020**, *8*, 8848−8856.
(50) Wang, N.; Zhao, K.; Ding, T.; Liu, W.; Ahmed, A. S.; Wang, Z.; Tian, M.; Sun, X. W.; Zhang, Q. Improving Interfacial Charge Recombination in Planar Heterojunction Perovskite Photovoltaics with Small Molecule as Electron Transport Layer. *Adv. Energy Mater.* **2017**, *7*, 1700522.
(51) Liu, K.; Dai, S.; Meng, F.; Shi, J.; Li, Y.; Wu, J.; Meng, Q.; Zhan, X. Fluorinated Fused Nonacyclic Interfacial Materials for Efficient and Stable Perovskite Solar Cells. *J. Mater. Chem. A* **2017**, *5*, 21414−21421.
(52) Fang, R.; Wu, S.; Chen, W.; Liu, Z.; Zhang, S.; Chen, R.; Yue, Y.; Deng, L.; Cheng, Y.-B.; Han, L.; Chen, W. [6, 6]-Phenyl-C61-Butyric Acid Methyl Ester/Cerium Oxide Bilayer Structure as Efficient and Stable Electron Transport Layer for Inverted Perovskite Solar Cells. *ACS Nano* **2018**, *12*, 2403−2414.
(53) Abdi-Jalebi, M.; Dar, M. I.; Senanayak, S. P.; Sadhanala, A.; Andaji-Garmaroudi, Z.; Pazos-Outón, L. M.; Richter, J. M.; Pearson, A. J.; Sirringhaus, H.; Grätzel, M.; Friend, R. H. Charge Extraction via Graded Doping of Hole Transport Layers Gives Highly Luminescent and Stable Metal Halide Perovskite Devices. *Sci. Adv.* **2019**, *5*, No. eaav2012.
(54) Kim, J.; Godin, R.; Dimitrov, S. D.; Du, T.; Bryant, D.; McLachlan, M. A.; Durrant, J. R. Excitation Density Dependent Photoluminescence Quenching and Charge Transfer Efficiencies in Hybrid Perovskite/Organic Semiconductor Bilayers. *Adv. Energy Mater.* **2018**, *8*, 1802474.
(55) Docampo, P.; Ball, J. M.; Darwich, M.; Eperon, G. E.; Snaith, H. J. Efficient Organometal Trihalide Perovskite Planar-Heterojunction Solar Cells on Flexible Polymer Substrate. *Nat. Commun.* **2013**, *9*, 395−398.
(56) Krückemeier, L.; Krogmeier, B.; Liu, Z.; Rau, U.; Kirchartz, T. Understanding Transient Photoluminescence in Halide Perovskite Layer Stacks and Solar Cells. *Adv. Energy Mater.* **2021**, *11*, 2003489.
(57) Shao, Y.; Xiao, Z.; Bi, C.; Yuan, Y.; Huang, J. Origin and Elimination of Photocurrent Hysteresis by Fullerene Passivation in

https://doi.org/10.1021/acsaem.1c02913
ACS Appl. Energy Mater. XXXX, XXX, XXX−XXX

CH3NH3PbI3 Planar Heterojunction Solar Cells. *Nat. Commun.* **2014**, *5*, 5784.
(58) Muduli, S.; Pandey, P.; Devatha, G.; Babar, R.; Kothari, D. C.; Kabir, M.; Pillai, P. P.; Ogale, S. Photoluminescence Quenching in Self-Assembled CsPbBr3 Quantum Dots on Few-Layer Black Phosphorus Sheets. *Angew. Chem.* **2018**, *130*, 7808−7812.
(59) Zhang, W.; Wan, L.; Li, X.; Wu, Y.; Fu, S.; Fang, J. A Dopant-Free Polyelectrolyte Hole-Transport Layer for High Efficiency and Stable Planar Perovskite Solar Cells. *J. Mater. Chem. A* **2019**, *7*, 18898−18905.
(60) Deng, L.-L.; Zhan, X.-X.; Lin, J.-W.; Ho, R.-M.; Zheng, L.-S.; Xie, S.-Y. Isomer-Dependent Photovoltaic Properties of the [6, 6]-Phenyl-C61 (or C71)-Butyric Acid Methyl Esters. *Sol. RRL* **2021**, *5*, 2000816.
(61) Stolterfoht, M.; Caprioglio, P.; Wolff, C. M.; Márquez, J. A.; Nordmann, J.; Zhang, S.; Rothhardt, D.; Hörmann, U.; Amir, Y.; Redinger, A.; et al. The Impact of Energy Alignment and Interfacial Recombination on the Internal and External Open-Circuit Voltage of Perovskite Solar Cells. *Energy Environ. Sci.* **2019**, *12*, 2778−2788.
(62) Kirchartz, T.; Márquez, J. A.; Stolterfoht, M.; Unold, T. Photoluminescence-Based Characterization of Halide Perovskites for Photovoltaics. *Adv. Energy Mater.* **2020**, *10*, 1904134.
(63) Patil, P.; Mann, D. S.; Nakate, U. T.; Hahn, Y.-B.; Kwon, S.-N.; Na, S.-I. Hybrid Interfacial ETL Engineering using PCBM-SnS2 for High-Performance PIN Structured Planar Perovskite Solar Cells. *Chem. Eng. J.* **2020**, *397*, 125504.
(64) Mann, D. S.; Seo, Y.-H.; Kwon, S.-N.; Na, S.-I. Efficient and Stable Planar Perovskite Solar Cells with a PEDOT: PSS/SrGO Hole Interfacial Layer. *J. Alloys Compd.* **2020**, *812*, 152091.
(65) Subedi, B.; Song, Z.; Chen, C.; Li, C.; Ghimire, K.; Junda, M. M.; Subedi, I.; Yan, Y.; Podraza, N. J. Optical and Electronic Losses Arising from Physically Mixed Interfacial Layers in Perovskite Solar Cells. *ACS Appl. Mater. Interfaces* **2021**, *13*, 4923−4934.
(66) Shao, S.; Dong, J.; Duim, H.; Gert, H.; Blake, G. R.; Portale, G.; Loi, M. A. Enhancing the Crystallinity and Perfecting the Orientation of Formamidinium Tin Iodide for Highly Efficient Sn-based Perovskite Solar Cells. *Nano Energy* **2019**, *60*, 810−816.
(67) Lee, S.; Moon, J.; Ryu, J.; Parida, B.; Yoon, S.; Lee, D.-G.; Cho, J. S.; Hayase, S.; Kang, D.-W. Inorganic Narrow Bandgap $CsPb_{0.4}Sn_{0.6}I_{2.4}Br_{0.6}$ Perovskite Solar Cells with Exceptional Efficiency. *Nano Energy* **2020**, *77*, 105309.
(68) Gonzalez-Pedro, V.; Juarez-Perez, E. J.; Arsyad, W.-S.; Barea, E. M.; Fabregat-Santiago, F.; Mora-Sero, I.; Bisquert, J. General Working Principles of CH3NH3PbX3 Perovskite Solar Cells. *Nano Lett.* **2014**, *14*, 888−893.

https://doi.org/10.1021/acsaem.1c02913
ACS Appl. Energy Mater. XXXX, XXX, XXX−XXX